# Investigation of level structure in the semimagic nucleus $^{91}$Nb and systematics of nuclear structure characteristics near $A = 90$

Yi-Heng Wu,[1,2] Jing-Bin Lu,[1,*] Zhen Ren,[1] Tian-Jiao Gao,[1] Pei-Yao Yang,[1] Yan Hao,[1] Guan-Jian Fu,[3] Jian Li,[1] Ke-Yan Ma,[1] Xiao-Guang Wu,[4] Yun Zheng,[4] and Cong-Bo Li[4]

[1]*College of Physics, Jilin University, Changchun 130012, China*
[2]*School of Electronic Engineering and Intelligent Manufacturing, AnQing Normal University, Anqing 246133, China*
[3]*School of Physics Science and Engineering, Tongji University, Shanghai 200092, China*
[4]*China Institute of Atomic Energy, Beijing 102413, China*

(Received 10 August 2022; revised 23 August 2022; accepted 9 November 2022; published 30 November 2022)

We report the new level scheme of the $^{91}$Nb nucleus established by the reactions $^{82}$Se($^{14}$N, $5n$)$^{91}$Nb and $^{76}$Ge($^{19}$F, $4n$)$^{91}$Nb. Thirty new transitions with energies up to about 12 MeV are assigned to the $^{91}$Nb nucleus and placed in the proposed level scheme. The excited levels are well reproduced by shell-model calculations with the GWBXG effective interaction. The obtained results, which conform to the most experimental data well, manifest that the high spins are construed as the proton excitations from $1p_{3/2}$, $0f_{5/2}$, and $1p_{1/2}$ orbitals, to the $0g_{9/2}$ orbital with the breakup of the $Z = 38$ (40) core, as well as neutron excitations from the $0g_{9/2}$ orbital to the $1d_{5/2}$ or $0g_{7/2}$ orbital with the breakup of the $N = 50$ core.

DOI: 10.1103/PhysRevC.106.054326

## I. INTRODUCTION

The investigations of level structures in nuclei with proton $Z \approx 40$ and neutron $N \approx 50$ remain a rewarding work, which provided valuable information to explore the usability of the shell model, especially in high spin levels. The $N = 50$ nuclei, $^{89}$Y [1–3], $^{90}$Zr [4–6], $^{91}$Nb [7–9], $^{92}$Mo [10–13], $^{93}$Tc [14–16], and $^{94}$Ru [17–19], have several valence protons above the $Z = 38$ ($Z = 40$) subshell. The low spin levels were well elaborated within the shell-model framework, taking into account proton-hole excitations from the $pfg$ shells ($1p_{3/2}, 0f_{5/2}, 1p_{1/2}, 0g_{9/2}$). The inclusion of neutron core excitation across the $N = 50$ shell closure was imperative to fully explain the generation mechanisms for the high spin or high excitation energy levels.

The previous researches of the $N = 50$ nuclei $^{89}$Y, $^{90}$Zr, $^{93}$Tc, and $^{94}$Ru display strong $E2$ transitions at low or even moderate spin states, which result from a recoupling of the pure protons in the $pfg$ shells ($1p_{3/2}$, $0f_{5/2}$, $1p_{1/2}$, $0g_{9/2}$). The higher spin levels display strong $M1$ transitions, which are attributed to proton excitation from the $pf$ shells ($1p_{3/2}$, $0f_{5/2}$, $1p_{1/2}$) to the $g_{9/2}$ orbit, coupling to a neutron excitation from the $g_{9/2}$ orbit to the $d_{5/2}$ orbit. One might expect that the strong $M1$ and $E2$ transitions would be consistently predicted in the $^{91}$Nb nucleus by employing these ideas. It is therefore of worth to investigate systematically the $N = 50$ nuclei and explore the possible mechanisms for generating these states. The low-lying levels of the $^{91}$Nb nucleus were investigated using $^{91}$Zr($p$, $n\gamma$)$^{91}$Nb, $^{90}$Zr($\alpha$, $t$)$^{91}$Nb, and $^{88}$Sr($^{6}$Li, $p2n$)$^{91}$Nb [20–23]. The high spin levels of the $^{91}$Nb nucleus, as structured through the $^{82}$Se ($^{14}$N, $5n$) $^{91}$Nb reaction [7], were established up to the energy level of about 10 MeV. To extend our knowledge on the effects of the $Z = 38$ ($Z = 40$) subshell and $N = 50$ closed shell on the level structures, we have reinvestigated high spin states in the $^{91}$Nb nucleus. As a part of systematic studies of the level structures in the $A \approx 90$ ($Z \approx 38$, $N \approx 50$) mass region, further researches on the level structure of the $^{91}$Nb nucleus would offer a comparison with the known nuclear structure systematics of this mass region and promote verification of the shell model, invoked for in-depth explication of the experimental observations.

## II. EXPERIMENTS AND RESULTS

High spin levels in the $^{91}$Nb nucleus were produced following the $^{82}$Se($^{14}$N, $5n$)$^{91}$Nb reaction with a 54-MeV $^{14}$N beam provided by the HI-13 tandem accelerator at the China Institute of Atomic Energy in Beijing. The target thickness is 0.99 mg/cm$^2$ with 90% enriched $^{82}$Se and a backing of Yb foil of thickness 8.27 mg/cm$^2$. At the beginning of the experiment, the energy and efficiency calibrations of the detectors were performed by employing $^{60}$Co, $^{133}$Ba, and $^{152}$Eu standard sources covering the energy region from 39.52 keV ($^{152}$Eu) to 1408 keV ($^{152}$Eu). The more delicate energy calibrations were performed with characteristic $\gamma$ rays of the residual nuclei ($^{91}$Nb, $^{92}$Nb, and $^{89}$Y). In order to more precisely extract calibration coefficients, the whole energy range was divided into three regions, i.e., low, intermediate, and high energy regions. For the low and medium energy regions, the 148.2-, 327.8-, 356.0-, 471.0-, 560.0-, 711.2-, 762.5-, and 819.2-keV $\gamma$ rays were chosen, and the 762.5-, 819.2-, 1239.5-, 1657.6-, 2086.9-, and 2290.4-keV $\gamma$ rays were chosen for the high energy region

*ljb@jlu.edu.cn

 

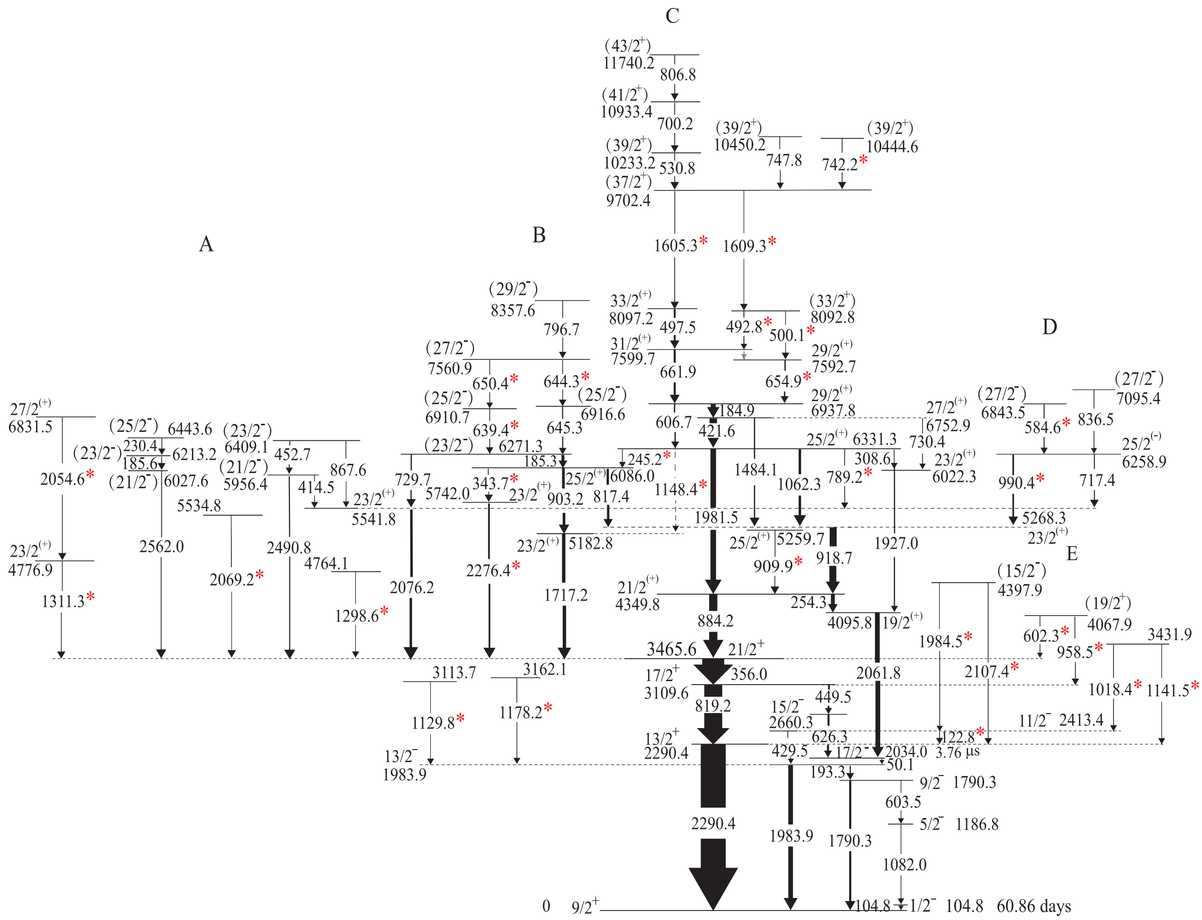


FIG. 1. Level scheme of the $^{91}$Nb nucleus from this paper and previous work [7]; the energies are labeled in keV. Newly identified $\gamma$ rays are labeled with red asterisks. The spin assignments for low-lying states are taken from Ref. [22]. The values of $T_{1/2}$ of the 104.8- and 2034.0-keV levels are adopted from Refs. [7,23]. The widths of the arrows represent the $\gamma$-ray relative intensities. The spin and parity assignments are tentative.

(above, these $\gamma$ rays originate from $^{91}$Nb, $^{92}$Nb, and $^{89}$Y nuclei).

A total of about $300 \times 10^6$ $\gamma$-$\gamma$ coincidence events were accumulated and sorted into two-dimensional symmetrized $E\gamma$-$E\gamma$ coincidence matrices. The asymmetrized $\gamma$-ray angular distribution from oriented nuclei (ADO) matrices were constructed by sorting the detectors located at $\approx 40^\circ$ (or $140^\circ$) and $\approx 90^\circ$, on one axis, whereas on the other they were from all the detectors. The spins of the levels were obtained by ADO ratios with the expression $I_\gamma$ (at $\approx 40^\circ$)/$I_\gamma$ (at $\approx 90^\circ$) [24]. With this expression, the corresponding ADO values for stretched quadrupole and dipole radiations are about 1.6 and 0.7, respectively. However, uncertainties occur for the spin assignments through analyzing ADO values, which are intermediate between these two cases. Moreover, the stretched quadrupole $\gamma$ rays cannot be differentiated from $\Delta I = 0$ dipole transitions or certain $E2/M1$ admixtures of $\Delta I = 1$ transitions. In these cases, the crossover or parallel transitions and their branching ratios can be regarded as the assistant means for the spin assignments.

For more information on energy levels, especially in the higher spin levels, the $^{76}$Ge ($^{19}$F, $4n$) $^{91}$Nb reaction was also utilized to populate the excited states of the $^{91}$Nb nucleus. The target consisted of a 2.22-mg/cm$^2$ foil of $^{76}$Ge (isotopically enriched to 96%) evaporated on the 10.0-mg/cm$^2$ lead backing.

As displayed in Fig. 1, the new level scheme of the $^{91}$Nb nucleus, as deduced from the current experiments, is extended up to the energy of about 12 MeV with the addition of 30 $\gamma$ rays to that reported earlier [7]. To facilitate discussions, the level scheme is divided roughly into five parts, which are marked A, B, C, D, and E. The positions of $\gamma$ rays in the new level scheme are based on their coincidence relationships, energy summings, and intensity balances. Relative intensities, $\gamma$-ray energies, ADO values, and proposed spin-parity assignments are exhibited in Tables I and II. The prompt coincidence spectra gated on the $\gamma$ rays from the $^{91}$Nb nucleus are exhibited in Figs. 2–4. In the following, the experimental results will be discussed in detail.

In the part marked A of Fig. 1, the new $\gamma$ rays with energies of 1298.6, 1311.3, 2054.6, and 2069.2 keV belonging to the $^{91}$Nb nucleus are confirmed to be in coincidence with the existing sequence of 356.0-, 819.2-, and 2290.4-keV transitions, but not with the 884.2-, 1717.2-, and 2076.2-keV

TABLE I. $\gamma$-ray energy (keV) and corresponding ADO value, relative intensity, initial and final spins, as well as initial and final excitation energies (keV) obtained from the present experiment in the $^{91}$Nb nucleus (continued in Table II).

| $E_\gamma$ [a] | $I_\gamma$ [b] | $R_{ADO}$ | $E_i^\pi$ | $E_f^\pi$ | $J_i^\pi$ | $J_f^\pi$ |
|---|---|---|---|---|---|---|
| 7.0[c] | | | 7599.7 | 7592.7 | $31/2^{(+)}$ | $29/2^{(+)}$ |
| 50.1 | | | 2034.0 | 1983.9 | $17/2^-$ | $13/2^-$ |
| 104.8 | | | 104.8 | 0 | $1/2^-$ | $9/2^+$ |
| 122.8 | | | 2413.4 | 2290.4 | $11/2^-$ | $13/2^+$ |
| 184.9 | 27.7 (15) | 1.03 (12) | 6937.8 | 6752.9 | $29/2^{(+)}$ | $27/2^{(+)}$ |
| 185.3 | 13.47 (59) | 0.96 (16) | 6271.3 | 6086.0 | $(23/2^-)$ | $25/2^{(+)}$ |
| 185.6 | | | 6213.2 | 6027.6 | $(23/2^-)$ | $(21/2^-)$ |
| 193.3 | | | 1983.9 | 1790.3 | $13/2^-$ | $9/2^-$ |
| 230.4 | 2.35 (40) | | 6443.6 | 6213.2 | $(25/2^-)$ | $(23/2^-)$ |
| 245.2 | | | 6331.3 | 6086.0 | $25/2^{(+)}$ | $25/2^{(+)}$ |
| 254.3 | 17.70 (36) | 1.01 (5) | 4349.8 | 4095.8 | $21/2^{(+)}$ | $19/2^{(+)}$ |
| 308.6 | 2.71 (35) | 0.51 (14) | 6331.3 | 6022.3 | $25/2^{(+)}$ | $23/2^{(+)}$ |
| 343.7 | 3.15 (29) | 0.96 (17) | 6086.0 | 5742.0 | $25/2^{(+)}$ | $23/2^{(+)}$ |
| 356.0 | 100 | 1.65(6) | 3465.6 | 3109.6 | $21/2^+$ | $17/2^+$ |
| 414.5 | $<2$ | | 5956.4 | 5541.8 | $(21/2^-)$ | $23/2^{(+)}$ |
| 421.6 | 33.9 (23) | 0.68 (5) | 6752.9 | 6331.3 | $27/2^{(+)}$ | $25/2^{(+)}$ |
| 429.5 | | | 2413.4 | 1983.9 | $11/2^-$ | $13/2^-$ |
| 449.5 | 7.91 (29) | 0.98 (8) | 3109.6 | 2660.3 | $17/2^+$ | $15/2^-$ |
| 452.7 | 4.03 (25) | 0.58 (6) | 6409.1 | 5956.4 | $(23/2^-)$ | $(21/2^-)$ |
| 492.8 | 4.32 (19) | | 8092.8 | 7599.7 | $(33/2^+)$ | $31/2^{(+)}$ |
| 497.5 | 8.61 (27) | 0.81 (16) | 8097.2 | 7599.7 | $33/2^{(+)}$ | $31/2^{(+)}$ |
| 500.1 | | | 8092.8 | 7592.7 | $(33/2^+)$ | $29/2^{(+)}$ |
| 530.8 | | | 10233.2 | 9702.4 | $(39/2^+)$ | $(37/2^+)$ |
| 584.6 | 4.14 (48) | | 6843.5 | 6258.9 | $(27/2^-)$ | $25/2^{(-)}$ |
| 602.3 | | | 4067.9 | 3465.6 | $(19/2^+)$ | $21/2^+$ |
| 603.5 | | | 1790.3 | 1186.8 | $9/2^-$ | $5/2^-$ |
| 606.7 | 6.01 (35) | 1.58 (15) | 6937.8 | 6331.3 | $29/2^{(+)}$ | $25/2^{(+)}$ |
| 626.3 | 9.07 (36) | 0.95 (8) | 2660.3 | 2034.0 | $15/2^-$ | $17/2^-$ |
| 639.4 | | | 6910.7 | 6271.3 | $(25/2^-)$ | $(23/2^-)$ |
| 644.3 | | | 7560.9 | 6916.6 | $(27/2^-)$ | $(25/2^-)$ |
| 645.3 | 4.90 (90) | 0.79 (9) | 6916.6 | 6271.3 | $(25/2^-)$ | $(23/2^-)$ |
| 650.4 | | | 7560.9 | 6910.7 | $(27/2^-)$ | $(25/2^-)$ |
| 654.9 | 6.07 (26) | 1.45 (13) | 7592.7 | 6937.8 | $29/2^{(+)}$ | $29/2^{(+)}$ |
| 661.9 | 9.03 (31) | 0.69 (9) | 7599.7 | 6937.8 | $31/2^{(+)}$ | $29/2^{(+)}$ |
| 700.2 | | | 10933.4 | 10233.2 | $(41/2^+)$ | $(39/2^+)$ |
| 717.4 | 4.36 (29) | 0.92 (23) | 6258.9 | 5541.8 | $25/2^{(-)}$ | $23/2^{(+)}$ |
| 729.7 | 5.43 (40) | 1.37 (8) | 6271.3 | 5541.8 | $(23/2^-)$ | $23/2^{(+)}$ |
| 730.4 | 1.90 (32) | | 6752.9 | 6022.3 | $27/2^{(+)}$ | $23/2^{(+)}$ |
| 742.2 | | | 10444.6 | 9702.4 | $(39/2^+)$ | $(37/2^+)$ |
| 747.8 | 2.99 (18) | 0.69 (13) | 10450.2 | 9702.4 | $(39/2^+)$ | $(37/2^+)$ |
| 789.2 | 1.34 (33) | 0.92 (11) | 6331.3 | 5541.8 | $25/2^{(+)}$ | $23/2^{(+)}$ |
| 796.7 | 2.10 (20) | 0.85 (12) | 8357.6 | 7560.9 | $(29/2^-)$ | $(27/2^-)$ |
| 806.8 | | | 11740.2 | 10933.4 | $(43/2^+)$ | $(41/2^+)$ |
| 817.4 | 10.65 (92) | 1.05 (18) | 6086.0 | 5268.3 | $25/2^{(+)}$ | $23/2^{(+)}$ |
| 819.2 | 83.4 (25) | 1.64 (11) | 3109.6 | 2290.4 | $17/2^+$ | $13/2^+$ |
| 836.5 | $<2$ | | 7095.4 | 6258.9 | $(27/2^-)$ | $25/2^{(-)}$ |
| 867.6 | | | 6409.1 | 5541.8 | $(23/2^-)$ | $23/2^{(+)}$ |
| 884.2 | 37.1 (13) | 1.34 (10) | 4349.8 | 3465.6 | $21/2^{(+)}$ | $21/2^+$ |
| 903.2 | 11.98 (36) | 0.72 (4) | 6086.0 | 5182.8 | $25/2^{(+)}$ | $23/2^{(+)}$ |
| 909.9 | 3.29 (19) | 1.79 (23) | 5259.7 | 4349.8 | $25/2^{(+)}$ | $21/2^{(+)}$ |
| 918.7 | 31.61 (89) | 0.52 (5) | 5268.3 | 4349.8 | $23/2^{(+)}$ | $21/2^{(+)}$ |
| 958.5 | | | 4067.9 | 3109.6 | $(19/2^+)$ | $17/2^+$ |
| 990.4 | 7.32 (48) | 1.03 (16) | 6258.9 | 5268.3 | $25/2^{(-)}$ | $23/2^{(+)}$ |

[a]The uncertainty in strong $\gamma$-ray energies is less than 0.4 keV; for weak $\gamma$-ray energies, it is about 0.7 keV.
[b]Intensities are corrected for detector efficiency and normalized to 100 for the 356.0-keV $\gamma$ ray.
[c]It is unobserved but deduced from the coincidence relations.

TABLE II. Continued from Table I.

| $E_\gamma$ [a] | $I_\gamma$ [b] | $R_{ADO}$ | $E_i^\pi$ | $E_f^\pi$ | $J_i^\pi$ | $J_f^\pi$ |
|---|---|---|---|---|---|---|
| 1018.4 | | | 3431.9 | 2413.4 | | $11/2^-$ |
| 1062.3 | 11.34 (34) | 0.55 (8) | 6331.3 | 5268.3 | $25/2^{(+)}$ | $23/2^{(+)}$ |
| 1082.0 | | | 1186.8 | 104.8 | $5/2^-$ | $1/2^-$ |
| 1129.8 | | | 3113.7 | 1983.9 | | $13/2^-$ |
| 1141.5 | | | 3431.9 | 2290.4 | | $13/2^+$ |
| 1178.2 | | | 3162.1 | 1983.9 | | $13/2^-$ |
| 1298.6 | | | 4764.1 | 3465.6 | | $21/2^+$ |
| 1311.3 | 3.12 (41) | 1.07 (24) | 4776.9 | 3465.6 | $23/2^{(+)}$ | $21/2^+$ |
| 1484.1 | 5.64 (30) | 1.52 (19) | 6752.9 | 5268.3 | $27/2^{(+)}$ | $23/2^{(+)}$ |
| 1605.3 | | | 9702.4 | 8097.2 | $(37/2^+)$ | $33/2^{(+)}$ |
| 1609.3 | | | 9702.4 | 8092.8 | $(37/2^+)$ | $(33/2^+)$ |
| 1717.2 | 15.40 (59) | 0.91 (9) | 5182.8 | 3465.6 | $23/2^{(+)}$ | $21/2^+$ |
| 1790.3 | 9.71 (19) | 1.50 (5) | 1790.3 | 0.0 | $9/2^-$ | $9/2^+$ |
| 1927.0 | 5.23 (76) | | 6022.3 | 4095.8 | $23/2^{(+)}$ | $19/2^{(+)}$ |
| 1981.5 | 25.2 (11) | 1.33(18) | 6331.3 | 4349.8 | $25/2^{(+)}$ | $21/2^{(+)}$ |
| 1983.9 | 21.2 (14) | 2.20 (19) | 1983.9 | 0.0 | $13/2^-$ | $9/2^+$ |
| 1984.5 | | | 4397.9 | 2413.4 | $(15/2^-)$ | $11/2^-$ |
| 2054.6 | 3.10 (29) | 1.96 (38) | 6831.5 | 4776.9 | $27/2^{(+)}$ | $23/2^{(+)}$ |
| 2061.8 | 21.50 (73) | 1.02 (8) | 4095.8 | 2034.0 | $19/2^{(+)}$ | $17/2^-$ |
| 2069.2 | | | 5534.8 | 3465.6 | | $21/2^+$ |
| 2076.2 | 11.15 (36) | 1.03 (14) | 5541.8 | 3465.6 | $23/2^{(+)}$ | $21/2^+$ |
| 2107.4 | | | 4397.9 | 2290.4 | $(15/2^-)$ | $13/2^+$ |
| 2276.4 | 7.81 (97) | 1.05 (29) | 5742.0 | 3465.6 | $23/2^{(+)}$ | $21/2^+$ |
| 2290.4 | 113.2 (37) | 1.62 (15) | 2290.4 | 0.0 | $13/2^+$ | $9/2^+$ |
| 2490.8 | 4.90 (29) | 1.38 (31) | 5956.4 | 3465.6 | $(21/2^-)$ | $21/2^+$ |
| 2562.0 | 3.79 (13) | | 6027.6 | 3465.6 | $(21/2^-)$ | $21/2^+$ |

[a]The uncertainty in strong $\gamma$-ray energies is less than 0.4 keV; for weak $\gamma$-ray energies, it is about 0.7 keV.
[b]Intensities are corrected for detector efficiency and normalized to 100 for the 356.0-keV $\gamma$ ray.

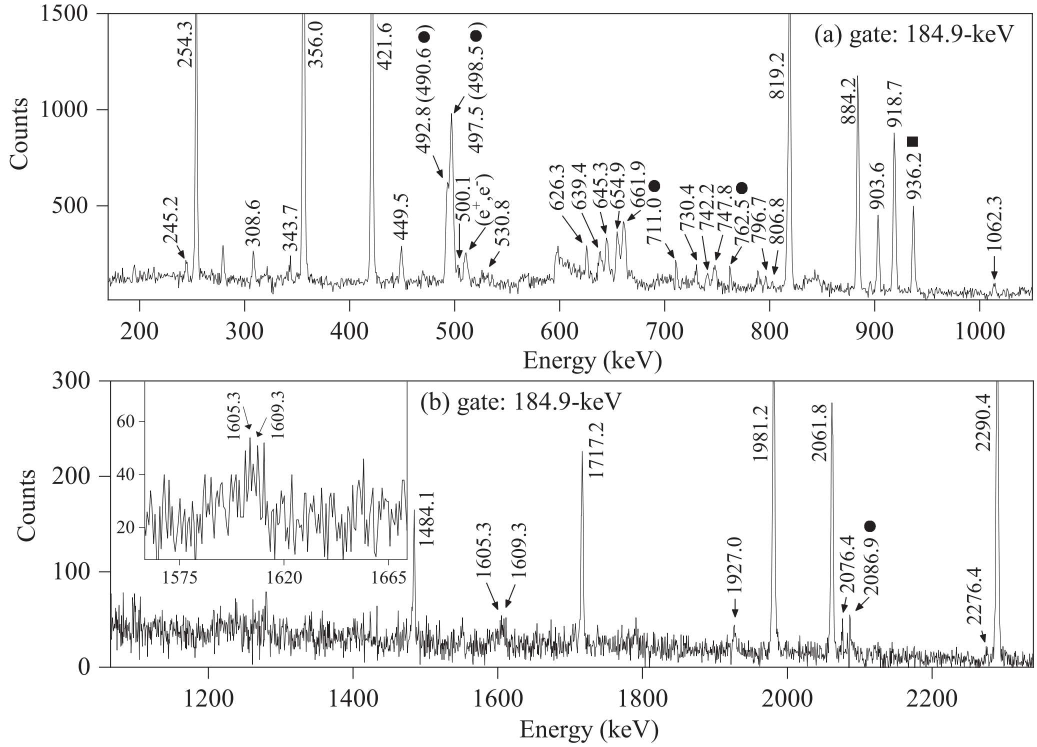


FIG. 2. Coincidence spectrum of $^{91}$Nb gated on (a, b) a 184.9-keV $\gamma$ ray. $\gamma$ rays are marked with their energies in keV. The peaks with black circles and squares are contaminated by the reactions $^{82}$Se ($^{14}$N, $4n$) $^{92}$Nb and $^{14}$N ($\alpha$, $\gamma$) $^{18}$F, respectively.

transitions. In addition, the 2054.6-keV transition is coincident with the 1311.3-keV transition. These $\gamma$ rays are located above the $21/2^+$ state (3465.5-keV level) as shown in Fig. 1. In consideration of their ADO values, we tentatively assign the $\Delta I = 2$ character for the 2054.4-keV $\gamma$ ray and $\Delta I = 1$ character for the 1311.3-keV $\gamma$ ray. These assignments make the identifications of $23/2^{(+)}$ and $27/2^{(+)}$ for the 4776.9- and 6831.5-keV levels, respectively. The 1298.6- and 2069.2-keV transitions are very weakly populated, and for that reason both the ADO values and intensities are not deduced.

In the part B of Fig. 1, the new transitions with energies of 343.7 and 2276.4 keV are assigned to connect the $25/2^{(+)}$ state (6086.0-keV level) and the $21/2^+$ state (3465.6-keV level). Based on their ADO values, both the 343.7- and 2276.4-keV $\gamma$ rays are designated as $\Delta I = 1$ character. The 245.2-keV $\gamma$ ray, as a linking transition, is placed between the $25/2^{(+)}$ state (6331.3-keV level) and the $25/2^{(+)}$ state (6086.0-keV level). Furthermore, above the $(23/2^-)$ state of 6271.3-keV level, the new $\gamma$ rays with 639.4, 644.3, and 650.4 keV are assigned in the present level scheme.

As for transitions in part C, above the $29/2^{(+)}$ state (6937.8-keV level), the known 661.9-, 497.5-, 530.8-, 700.2-, 747.8-, and 806.8-keV transitions, reported in Ref. [7], are confirmed in our experiments. The intensities and ADO values for 530.8-, 700.2-, and 806.8-keV $\gamma$ rays are not deduced because of poor data statistics. As a consequence, they are tentatively placed in the order shown in Fig. 1. The new transitions with 492.8-, 500.1-, 654.9-, 742.2-, 1605.3-, and 1609.3-keV energies are identified. The new transitions 492.8, 500.1, 654.9, 742.2, 1605.3, and 1609.3 keV are displayed in gated spectrum of the 184.9-keV $\gamma$ ray given in Fig. 2. However, the 654.9- and 500.1-keV transitions are not seen in the gated spectrum of the 661.9-keV $\gamma$ ray. Simultaneously, in the spectrum gated on the 492.8-keV $\gamma$ ray, the known 184.9-, 421.6-, 1981.5-, 884.2-, and 606.7-keV transitions, as well as the new transitions 654.9, 742.2, and 1609.3 keV, are observed and vice versa, while the 497.5-, 1605.3-, and 500.1-keV transitions are not observed. Between $31/2^{(+)}$ (7599.7-keV level) and $29/2^{(+)}$ (7592.7-keV level), there should be a 7.0-keV $\gamma$ ray deduced from coincidence relations, but we could not observe it because of the detection limit of the present experiment. In addition, a new $\gamma$ ray with the energy of 789.2 keV is placed on the $23/2^{(+)}$ state (5541.8-keV level). The 789.2-keV transition is proposed as $\Delta I = 1$ character, which is consistent with its measured ADO value of 0.92. Above the $21/2^{(+)}$ state at 4349.8-keV level, a new $\gamma$ ray with energy of 909.9 keV is placed on the $21/2^{(+)}$ state at 4349.8-keV level. The ADO value for the 909.9-keV $\gamma$ ray is about 1.79, and we tentatively assign the state at 5259.7 keV with a spin parity of $25/2^{(+)}$ in the present level scheme. It is notable that one can see several peaks (i.e., 490.6, 498.5, 711.0, 762.5, and 2087.1 keV) in the gated 184.9-keV $\gamma$-ray spectrum. Based on the present data analyses, we confirm that the 490.6-, 498.5-, 711.0-, 762.5-, and 2087.1-keV $\gamma$ rays from the $^{92}$Nb nucleus are also coincident with the 183.6-keV $\gamma$-ray, though, which were not observed in Ref. [25]. As for the part D, a new cascade of two $\gamma$ rays with energies of 584.6 and 990.4 keV is identified. Figures 3 and 4 present the spectra gated by the 990.4-, 918.7-, and 584.6-keV $\gamma$ rays. As illustrated in Fig. 3(a), the new transition 584.6 keV and the known transitions 254.3, 356.0, 884.2, 918.7, and 2061.8 keV are observed in the spectrum on the 990.4-keV $\gamma$ ray. The

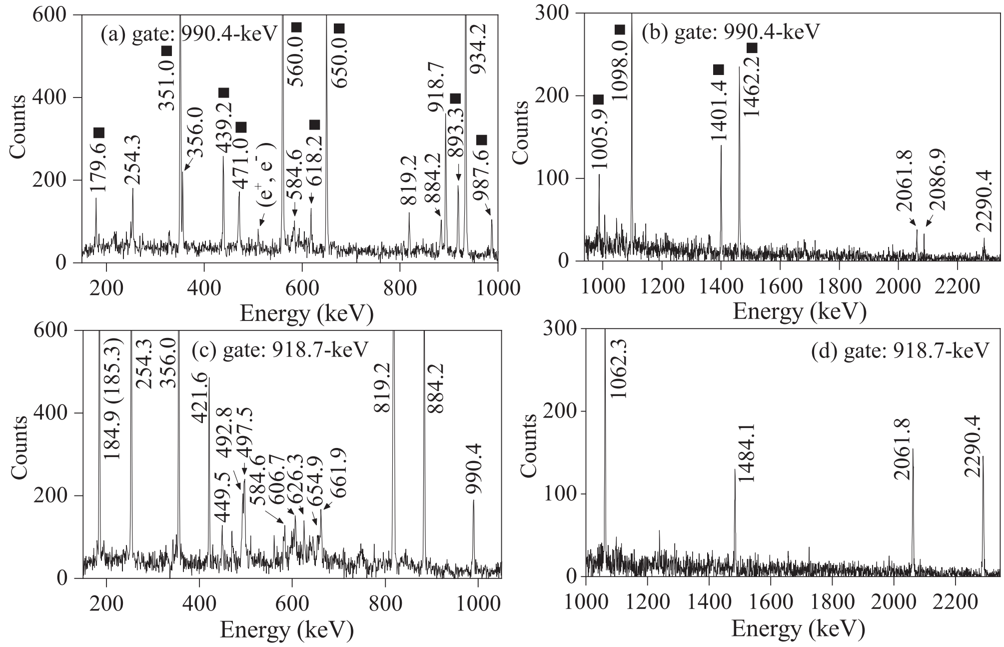


FIG. 3. Coincidence spectra of $^{91}$Nb gated on (a, b) a 990.4-keV $\gamma$ ray and (c, d) a 918.7-keV $\gamma$ ray. $\gamma$ rays are marked with their energies in keV. The peaks with black squares are contaminated by the reactions $^{82}$Se ($^{14}$N, $1p3n$) $^{92}$Zr.

new transitions 990.4 and 584.6 keV are also observed in the gated spectrum of the known 918.7-keV $\gamma$ ray, as shown in Fig. 3(b). In addition, in the coincidence spectrum gated on the 584.6-keV transition, the known 254.3-, 356.0-, 884.2-, and 918.7-keV transitions, as well as the new transition 990.4 keV, are observed. The ADO value for the 990.4-keV $\gamma$ ray is about 1.03. Moreover, the difference energy between the $25/2^{(-)}$ (6258.9-keV level) and $23/2^{(+)}$ (5268.3-keV level) states is almost equivalent to the observed 990.4-keV $\gamma$ ray. Considering the coincidence relationship between 990.4- and

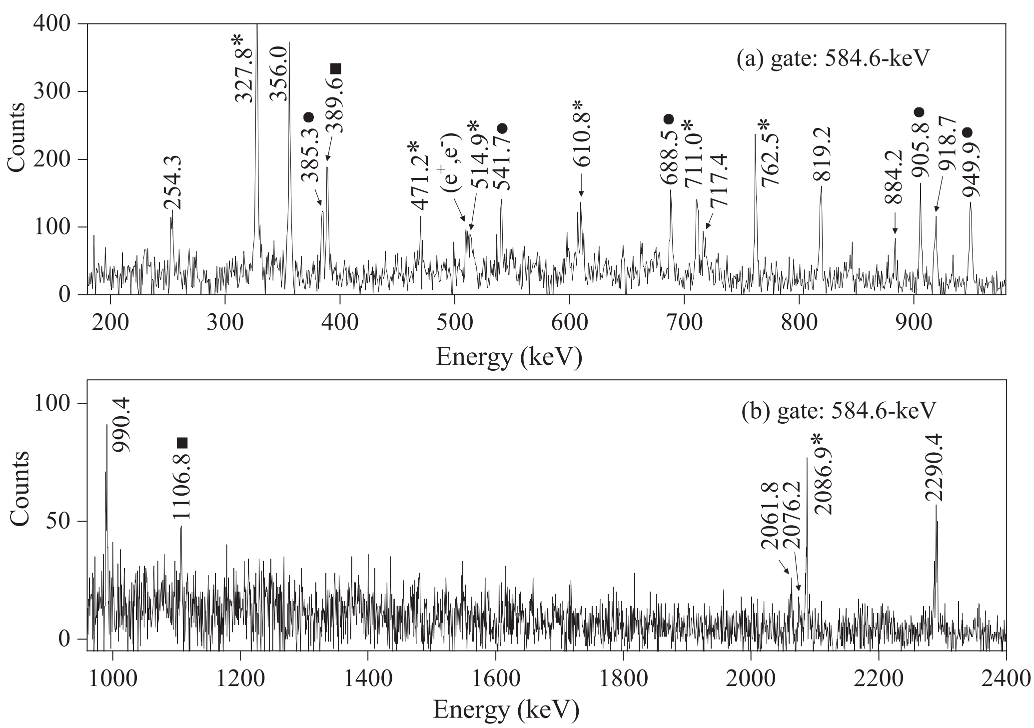


FIG. 4. Coincidence spectra of $^{91}$Nb gated on (a, b) a 584.6-keV $\gamma$ ray. $\gamma$ rays are labeled with their energies in keV. The peaks with single asterisks, black circles, and black squares are contaminated by the reactions $^{82}$Se ($^{14}$N, $4n$) $^{92}$Nb, $^{82}$Se ($^{14}$N, $3n$) $^{93}$Nb, and $^{82}$Se ($^{14}$N, $2p4n$) $^{90}$Y, respectively.

584.6-keV transitions, the ordering of these $\gamma$ rays is tentatively placed as shown in Fig. 1.

In the part E of Fig. 1, the 122.8-, 602.3-, 958.5-, 1018.5-, 1141.5-, 1984.5-, and 2107.5-keV transitions belonging to the $^{91}$Nb nucleus are added. The new transitions 1141.5 and 2107.5 keV are in coincidence with the 2290.4-keV $\gamma$ ray, which decay to the $13/2^+$ state (2290.4-keV level), but not with the 356.0-, 819.4-, and 449.5-keV transitions. The new $\gamma$ rays with energies of 2107.4 and 958.5 keV as well as the 1141.5-keV $\gamma$ rays are almost equal to the sum energies of 1984.5 and 122.8, 356.0 and 602.3, and 1018.4 and 122.8 keV, respectively. Considering the energy summings and coincidence relationships, these $\gamma$ rays are tentatively placed in the proposed level scheme as represented in Fig. 1. In addition, the new 1129.8- and 1178.2-keV $\gamma$ rays belonging to the $^{91}$Nb nucleus are identified and found to be coincident with the 1983.9-, 193.3-, and 1790.3-keV transitions deexciting the $13/2^-$ state at 1983.9 keV, but not with the 429.5-keV transition deexciting the $11/2^-$ state at 2413.4 keV.

## III. SHELL-MODEL CALCULATIONS AND DISCUSSIONS

The $^{91}$Nb isotones $^{88}$Sr [26,27], $^{89}$Y [2], $^{92}$Mo [11], and $^{93}$Tc [14] as well as the isotopes $^{91-93}$Nb [7,25,28] have not been observed in the strong $E2$ transitions in high spin states so far, which indicates no appreciable collectivity. The shell-model calculations for these nuclei show that neutron excitations across the $N = 50$ shell gap should be considered for the description of high spin states. On the proton side, excitations from the $1p0f$ orbits into the $0g_{9/2}$ orbit should be necessary for describing well the low and even medium spin states. To interpret the level structure from the present experiments, the shell-model calculation for the $^{91}$Nb nucleus is performed with proton and neutron core excitations across the $^{90}$Zr core; i.e., the valence proton holes are in the lower $f_{5/2}p_{3/2}p_{1/2}$ orbitals, the valence proton particles are in the upper $g_{9/2}$ orbital, the valence neutron holes are in the lower $g_{9/2}$ orbital, and the valence neutron particles are in the upper $d_{5/2}$ orbital. The shell-model calculations were performed with the NUSHELLX code [29]. The GWB model space is adopted with the GWBXG effective interaction. The single-particle states forming the GWB model space contains four proton orbits $\pi(f_{5/2},\ p_{3/2},\ p_{1/2},\ g_{9/2})$ and six neutron orbits $\nu(p_{1/2},\ g_{9/2},\ g_{7/2},\ d_{5/2},\ d_{3/2},\ s_{1/2})$ relative to an inert $^{66}$Ni core. The original two-body matrix elements (TMBEs) of the GWBXG interaction originate from bare G matrix of the H7B potential [30]. For the present G-matrix effective interaction, the 65 TMBEs for proton orbits are replaced with the values derived from Ref. [31]. The TMBEs between the $\pi(p_{1/2},\ g_{9/2})$ and the $\nu(d_{5/2},\ s_{1/2})$ orbits and that between the $\pi(p_{1/2},\ g_{9/2})$ and the $\nu(p_{1/2},\ g_{9/2})$ orbits are replaced with the values reported in Refs. [32,33]. The single particle energies are derived from Refs. [5,20]. In Refs. [5,20], one can see that the energy gap between the $f_{5/2}$ ($p_{1/2}$) and $g_{9/2}$ valence proton shells is 4.0 (2.7) MeV, and that the energy gap between the $g_{9/2}$ and $d_{5/2}$ valence neutrons shells is 4.4 MeV. These large energy gaps suggest a possible $Z = 38$ (40) subshell and $N = 50$ shell.

Figure 5 displays a comparison between the calculated energy levels employing GWBXG interactions and experimental ones from which it may be stated clearly that these calculations can reasonably describe the experimental energy levels. Main configuration components are listed in Tables III and IV, and comparison between experimental transition probabilities and calculation ones is shown in Table V. In Table III, the ground state $9/2^+$ is dominated by the configuration $\pi g_{9/2}$. The calculated $13/2^+$ and $17/2^+$ yrast states are dominated by the excitation of protons from the $p_{1/2}$ orbit across the $Z = 40$ subshell to the $g_{9/2}$ orbit. Meanwhile, both of the two states also include the core excitations of protons from the $f_{5/2}$ orbit across the $Z = 38$ subshell into the $g_{9/2}$ orbit, which indicates the $\pi(p_{1/2},\ g_{9/2})$ model space may fail to explain adequately even the low-lying levels in this nucleus.

The level energies with $3400 < E_{\text{expt.}} < 6100$ keV (except for the $23/2_3^+$ and $23/2_5^+$ levels) are characterized by the pure proton configurations $\pi(p_{3/2}f_{5/2}p_{1/2})^{-2}g_{9/2}^3$. The calculated $B(E2;\ 21/2_1^+ \rightarrow 17/2_1^+)$ value is $100.7e^2fm^4$, which is pretty close to the experimental value $(106 \pm 11)$ $e^2fm^4$ given in Ref. [9] (see Table V). The $23/2_3^+$ state arises from the coupling of an unpaired proton in the $g_{9/2}$ orbit and neutron core excited from the $g_{9/2}$ orbit to the empty $d_{5/2}$ orbit, viz., configuration of the form $\pi g_{9/2} \otimes \nu g_{9/2}^{-1}d_{5/2}$. The $23/2_5^+$ state comes from proton excitation from the $f_{5/2}p_{1/2}$ orbits to the $g_{9/2}$ orbit coupling to neutron excitation from the $g_{9/2}$ orbit to the empty $d_{5/2}$ orbit, leading to the configuration $\pi(f_{5/2}^{-1}p_{1/2}^{-1})g_{9/2}^3 \otimes \nu g_{9/2}^{-1}d_{5/2}$. In the levels above $25/2_2^+$ ($E_{\text{expt.}} = 6086.0$ keV), neutron core excitations become very important. It seems that breakup of the $N = 50$ shell gap is preferable to exciting more protons with the increasing of angular momentum above the 6086.0-keV level. The states from $25/2_3^+$ (6331.3-keV level) to $41/2^+$ (10933.4-keV level) are interpreted as proton excitation from the $f_{5/2}p$ orbits to the $g_{9/2}$ orbital, coupling to a neutron excitation from the $g_{9/2}$ orbit to the $d_{5/2}$ orbit, i.e., configuration of the form $\pi(f_{5/2}p)^{-2}g_{9/2}^3 \otimes \nu g_{9/2}^{-1}d_{5/2}$. The $43/2^+$ state (11740.2-keV level) is described mainly by proton excitation from the $f_{5/2}p$ orbits to the $g_{9/2}$ orbits, coupling a neutron excitation across the $N = 50$ shell closure to the $g_{7/2}$ orbit.

As mentioned, the electric quadrupole transitions $21/2_1^+ \rightarrow 17/2_1^+$, $17/2_1^+ \rightarrow 13/2_1^+$, and $13/2_1^+ \rightarrow 9/2_1^+$ are interpreted as proton excitation $f_{5/2}p \rightarrow g_{9/2}$. The calculations $B(E2)$ values are 100.7, 287.8, and 152.9 $e^2fm^4$, respectively. Similar characteristics, as reported in $N = 50$ isotones [3,14], were interpreted as the recouplings of the $\pi(g_{9/2})^n$ parts of configurations with $\Delta I = 2$. However, for the transitions $23/2_4^+ \rightarrow 19/2_2^+$ and $25/2_3^+ \rightarrow 21/2_2^+$, the calculations predict $B(E2)$ values decrease abruptly. The difference could be due to the forbidden $23/2_4^+ \rightarrow 19/2_2^+$ and $25/2_3^+ \rightarrow 21/2_2^+$ transitions from neutron core excited to pure proton states, whereas rather strong $M1$ transitions $31/2_1^+ \rightarrow 29/2_1^+$ and $33/2_1^+ \rightarrow 31/2_1^+$, the $B(M1)$ values of which are in the range of 1.1–2.6 $\mu_N^2$, are ascribed to the recouplings of the two unpaired neutrons, i.e., the $g_{9/2}$ neutron hole and the $d_{5/2}$ neutron. In other words, these enhanced $M1$ transitions might be regarded as a testimony for neutron core excitation.

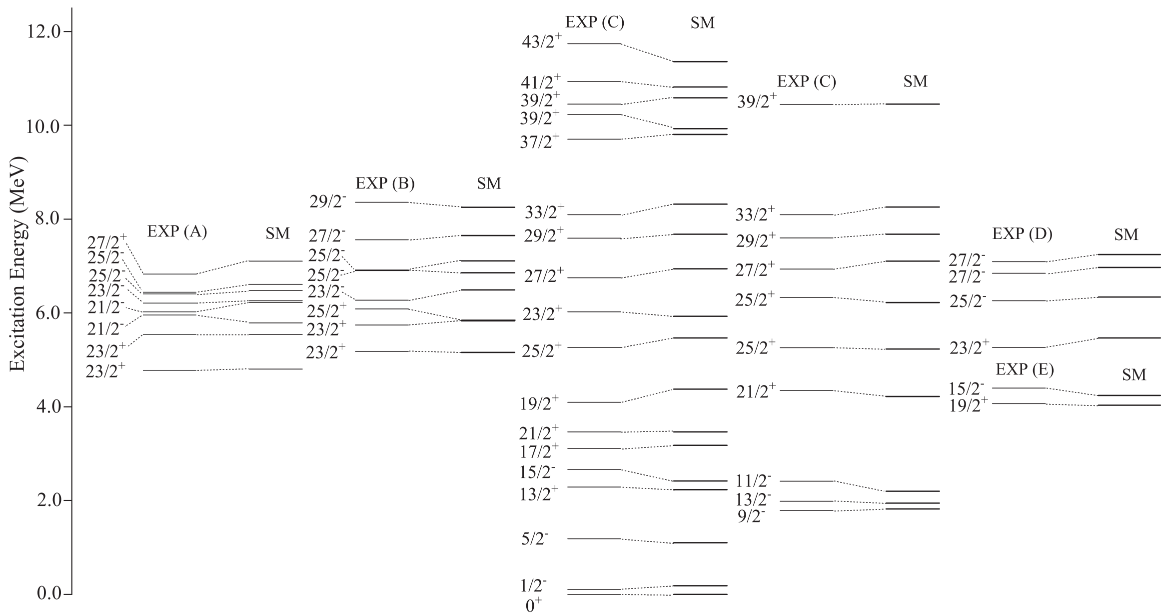


FIG. 5. Comparing of the experimental and calculated levels of the $^{91}$Nb nucleus.

The negative-parity states up to the $17/2^-$ state at 2034.0 keV are built from breaking one proton pair in the $p_{1/2}$ orbit and lifting one proton to the $g_{9/2}$ orbit, leading to the configuration $\pi p_{1/2}^{-1} g_{9/2}^2$. The only exception is the $15/2_2^-$ state at 4397.7 keV, which in the calculation arises from the proton excitation from the $f_{5/2}p_{1/2}$ orbit to the $g_{9/2}$ orbit, viz., configuration of the form $\pi(f_{5/2}^{-1}p_{1/2}^{-2})g_{9/2}^4$. Besides that, the $B(E2)$ strengths of the transitions $17/2_1^- \to 13/2_1^-$, $13/2_1^- \to 9/2_1^-$, and $9/2_1^- \to 5/2_1^-$ were also calculated. The corresponding calculated $B(E2)$ values are 37.2, 115.6, and 194.5 $e^2 fm^4$ respectively, which conformed well to the experimental ones in Ref. [2]. The $21/2_1^-$, $21/2_2^-$, and $23/2_1^-$ states arise from the excitation of protons across the $Z = 38$ subshell, leading to the configuration $\pi(p_{3/2}f_{5/2}p_{1/2})^{-3}g_{9/2}^4$. The $23/2_2^- \leqslant I^\pi \leqslant 29/2^-$ states are characterized as configuration $\pi(p_{3/2}f_{5/2}p_{1/2})^{-1}g_{9/2}^2 \otimes \nu g_{9/2}^{-1}d_{5/2}$.

## IV. SYSTEMATIC CHARACTERISTICS AROUND THE $A = 90$ REGION

The energies of the first $2^+$ states for even-even nuclei from Zr ($Z = 40$) to Cd ($Z = 48$) as well as the first $13/2^+$ states for odd-$A$ nuclei from Nb ($Z = 41$) to In ($Z = 49$) are illustrated in Figs. 6(a) and 6(c), respectively. A noteworthy feature of the excitation energies of $2^+$ ($13/2^+$) states in $^{90}$Zr ($^{91}$Nb) and $^{96}$Zr ($^{97}$Nb) nuclei is that they are significantly higher than those of other Zr (Nb) isotopes, which reveals that $N = 56$ is a good subshell closure. It underscores that the $^{96}$Zr nucleus has a high-lying $2^+$ state at 1750 keV, whereas the $2^+$ energies in $^{98}$Mo, $^{100}$Ru, $^{102}$Pd, and $^{104}$Cd nuclei are only 787, 540, 556, and 658 keV, respectively. The abrupt decrease in $2^+$ energies for the $N = 56$ isotones is incompatible with a spherical nucleus. Such disparate behavior with proton number $Z \geqslant 42$ may ascribe to the vanishing of the $N = 56$ neutron shell closure. Comparing with Zr and Mo, the Nb

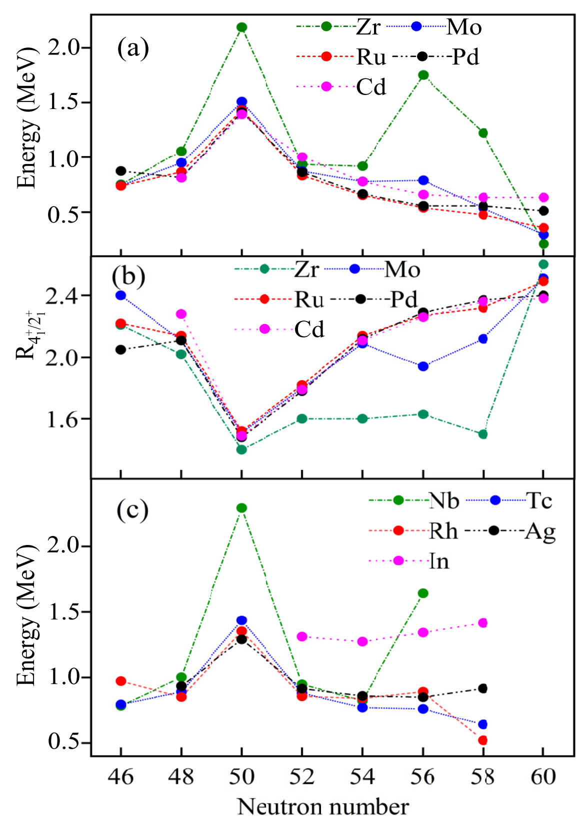


FIG. 6. (a) The evolution of the first $2^+$ states for $N = 46$–60: Zr (green circles) [4,34–36], Mo (blue circles) [13,37–39], Ru (red circles) [40–47], Pd (black circles) [41,44–51], and Cd (pink circles) [42–47,52,53] isotopes. (b) The ratio of the excitation energies of the first excited $4^+$ and $2^+$ states. (c) The evolution of the first $13/2^+$ states for $N = 46$–60: Nb (green circles) [54–60], Tc (blue circles) [55–61], Rh (red circles) [56–62], Ag (black circles) [57–63], and In (pink circles) [58–64].

TABLE III. Major components of configurations for the $^{91}$Nb nucleus. The configurations are formed by several components, where each component is of the form $p = [\pi(p(1), p(2), p(3), p(4)) \otimes \nu(n(1), n(2), n(3), n(4))]$, where $p(i)$ and $n(i)$ represent the proton number in ($f_{5/2}$, $p_{3/2}$, $p_{1/2}$, $g_{9/2}$) orbits and neutron number in ($p_{1/2}$, $g_{9/2}$, $g_{7/2}$, $d_{5/2}$) orbits, respectively (continued in Table IV).

| $I^\pi$ ($\hbar$) | $E_{exp}$ (keV) | $E_{cal}$ (keV) | Configurations $\pi \otimes \nu$ | Components (%) |
|---|---|---|---|---|
| $9/2^+$ | 0 | 0[a] | 6 4 2 1 ⊗ 2 10 0 0 | 59.3 |
| | | | 6 4 0 3 ⊗ 2 10 0 0 | 19.0 |
| | | | 6 2 2 3 ⊗ 2 10 0 0 | 13.4 |
| $13/2^+$ | 2290.4 | 2236[a] | 6 4 0 3 ⊗ 2 10 0 0 | 53.5 |
| | | | 4 4 2 3 ⊗ 2 10 0 0 | 16.9 |
| | | | 5 4 1 3 ⊗ 2 10 0 0 | 12.0 |
| $17/2^+$ | 3109.6 | 3179[a] | 6 4 0 3 ⊗ 2 10 0 0 | 62.0 |
| | | | 4 4 2 3 ⊗ 2 10 0 0 | 13.2 |
| $19/2_1^+$ | 4067.9 | 4069[a] | 5 4 1 3 ⊗ 2 10 0 0 | 51.1 |
| | | | 6 3 1 3 ⊗ 2 10 0 0 | 34.6 |
| $19/2_2^+$ | 4095.8 | 4378[a] | 5 4 1 3 ⊗ 2 10 0 0 | 62.0 |
| | | | 5 3 2 3 ⊗ 2 10 0 0 | 12.3 |
| $21/2_1^+$ | 3465.6 | 3468[a] | 6 4 0 3 ⊗ 2 10 0 0 | 68.6 |
| | | | 4 4 2 3 ⊗ 2 10 0 0 | 10.7 |
| $21/2_2^+$ | 4349.8 | 4274[a] | 5 4 1 3 ⊗ 2 10 0 0 | 84.1 |
| | | | 5 3 2 3 ⊗ 2 10 0 0 | 10.9 |
| $23/2_1^+$ | 4776.9 | 4807[a] | 5 4 1 3 ⊗ 2 10 0 0 | 82.5 |
| | | | 5 3 2 3 ⊗ 2 10 0 0 | 13.1 |
| $23/2_2^+$ | 5182.8 | 5160[b] | 5 4 1 3 ⊗ 2 10 0 0 | 53.1 |
| | | | 5 3 2 3 ⊗ 2 10 0 0 | 19.3 |
| $23/2_3^+$ | 5268.3 | 5469[b] | 6 4 2 1 ⊗ 2 9 0 1 | 46.7 |
| | | | 6 4 0 3 ⊗ 2 9 0 1 | 18.3 |
| | | | 6 2 2 3 ⊗ 2 9 0 1 | 10.2 |
| $23/2_4^+$ | 5541.8 | 5541[b] | 5 4 1 3 ⊗ 2 10 0 0 | 52.3 |
| | | | 6 3 1 3 ⊗ 2 10 0 0 | 23.7 |
| $23/2_5^+$ | 5742.0 | 5834[b] | 5 4 1 3 ⊗ 2 9 0 1 | 23.3 |
| | | | 6 4 0 3 ⊗ 2 9 0 1 | 20.2 |
| $23/2_6^+$ | 6022.3 | 5929[b] | 6 3 1 3 ⊗ 2 10 0 0 | 29.0 |
| | | | 5 3 2 3 ⊗ 2 10 0 0 | 26.5 |
| | | | 5 4 1 3 ⊗ 2 10 0 0 | 22.8 |
| $25/2_1^+$ | 5259.7 | 5229[b] | 5 4 1 3 ⊗ 2 10 0 0 | 74.8 |
| $25/2_2^+$ | 6086.0 | 5840[b] | 6 3 1 3 ⊗ 2 10 0 0 | 57.3 |
| | | | 5 3 2 3 ⊗ 2 10 0 0 | 12.3 |
| $25/2_3^+$ | 6331.3 | 6221[b] | 6 4 0 3 ⊗ 2 9 0 1 | 24.8 |
| | | | 5 4 1 3 ⊗ 2 9 0 1 | 23.7 |
| | | | 4 4 2 3 ⊗ 2 9 0 1 | 22.3 |
| $27/2_1^+$ | 6752.9 | 6943[b] | 5 4 1 3 ⊗ 2 9 0 1 | 28.8 |
| | | | 4 4 2 3 ⊗ 2 9 0 1 | 23.2 |
| $27/2_2^+$ | 6831.5 | 7103[b] | 6 4 0 3 ⊗ 2 9 0 1 | 34.7 |
| | | | 4 4 2 3 ⊗ 2 9 0 1 | 22.0 |
| $29/2_1^+$ | 6937.8 | 7107[b] | 6 4 0 3 ⊗ 2 9 0 1 | 42.8 |
| | | | 4 4 2 3 ⊗ 2 9 0 1 | 19.5 |
| $29/2_2^+$ | 7592.7 | 7679[b] | 5 4 1 3 ⊗ 2 9 0 1 | 61.1 |
| | | | 5 3 2 3 ⊗ 2 9 0 1 | 10.3 |
| $31/2_1^+$ | 7599.7 | 7678[b] | 5 4 1 3 ⊗ 2 9 0 1 | 71.0 |
| | | | 5 3 2 3 ⊗ 2 9 0 1 | 12.5 |
| $33/2_1^+$ | 8092.8 | 8256[b] | 5 4 1 3 ⊗ 2 9 0 1 | 73.4 |

TABLE III. (*Continued.*)

| $I^\pi$ ($\hbar$) | $E_{exp}$ (keV) | $E_{cal}$ (keV) | Configurations $\pi \otimes \nu$ | Components (%) |
|---|---|---|---|---|
| $33/2_2^+$ | 8097.2 | 8321[b] | 6 4 0 3 ⊗ 2 9 0 1 | 46.5 |
| | | | 4 4 2 3 ⊗ 2 9 0 1 | 15.5 |
| $37/2^+$ | 9702.4 | 9808[b] | 5 4 1 3 ⊗ 2 9 0 1 | 67.5 |

[a]Calculation with the model space $\pi(f_{5/2}, p_{3/2}, p_{1/2}, g_{9/2})$.
[b]$\pi(f_{5/2}, p_{3/2}, p_{1/2}, g_{9/2}) \otimes \nu(g_{9/2}, d_{5/2})$.

($Z = 41$) nucleus may be located at the transition between the region where the $N = 56$ subshell is active ($Z = 40$) and the open shell ($Z \geqslant 42$). As shown in Fig. 6(b), the $R_{4_1^+/2_1^+}$ values along the Mo, Ru, Pd, and Cd isotopic chains show similar tendency, but notable difference from the Zr isotopic chain. The ratio of reduced $R_{4_1^+/2_1^+}$ from $N = 60$ to 50, followed by a drop toward $N = 50$, is observed. Normally, an increase of collectivity is reflected by a drop of $2^+$ energies and a rise of $R_{4_1^+/2_1^+}$ towards the rotational limits. The $R_{4_1^+/2_1^+}$ values in $^{92}$Mo, $^{94}$Ru, $^{96}$Pd, and $^{98}$Cd as well as $^{90}$Zr, $^{92}$Zr, $^{94}$Zr, $^{96}$Zr, and $^{98}$Zr nuclei are around 1.5, which exhibited the typical characteristic of spherical nuclei. Figure 7(a) displays the first $2^+$ to $10^+$ levels of the $N = 50$ isotones from Zr ($Z = 40$) to Cd ($Z = 48$). As shown in Fig. 7(a), the excitation energies of $10^+$ states in $^{90}$Zr and $^{92}$Mo nuclei are significantly higher than those of other $N = 50$ isotones. The $10^+$ state in $^{90}$Zr arises from the excitation of protons from $f_{5/2}p_{1/2}$ orbits to the $g_{9/2}$ orbit, which has seniority $\nu = 4$ [5]. The $10^+$ state in $^{92}$Mo arises from the excitation of protons from $p_{1/2}$ orbits to

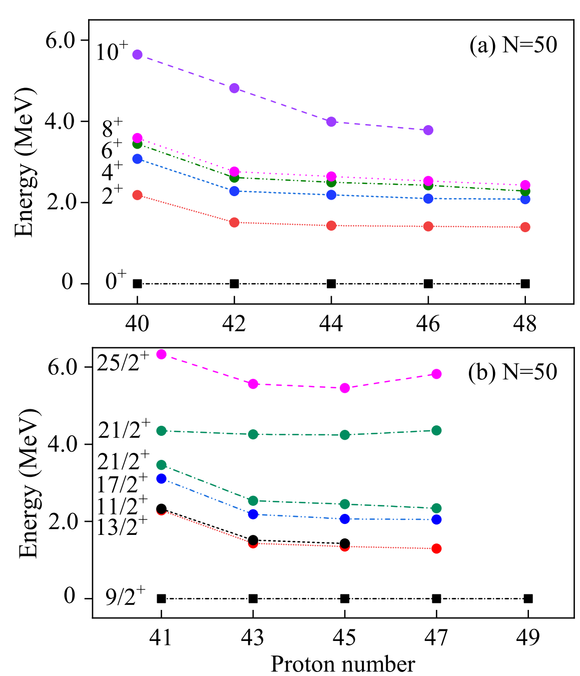


FIG. 7. (a) The evolution of positive parity states in even-even $N = 50$ isotones $^{90}$Zr [5], $^{92}$Mo [13], $^{94}$Ru [17], $^{96}$Pd [49], and $^{98}$Cd [51]. (b) The evolution of positive parity states in odd-$A$ $N = 50$ isotones $^{91}$Nb [7], $^{93}$Tc [15], $^{95}$Rh [58], and $^{97}$Ag [59].

TABLE IV. Continued from Table III.

| $I^\pi$ ($\hbar$) | $E_{exp}$ (keV) | $E_{cal}$ (keV) | Configurations $\pi \otimes \nu$ | Components (%) |
|---|---|---|---|---|
| $39/2_1^+$ | 10233.2 | 9927[b] | 5 4 1 3 ⊗ 2 9 0 1 | 75.5 |
| $39/2_2^+$ | 10444.6 | 10455[b] | 5 4 1 3 ⊗ 2 9 0 1 | 77.6 |
| $39/2_3^+$ | 10450.2 | 10820[b] | 5 4 1 3 ⊗ 2 9 0 1 | 65.4 |
| | | | 4 4 2 3 ⊗ 2 9 0 1 | 10.0 |
| $41/2^+$ | 10933.4 | 10589[b] | 5 4 1 3 ⊗ 2 9 0 1 | 80.0 |
| $43/2^+$ | 11740.2 | 11365[c] | 5 4 1 3 ⊗ 2 9 1 0 | 79.5 |
| | | | 5 3 2 3 ⊗ 2 9 1 0 | 13.1 |
| $1/2^-$ | 104.8 | 186[a] | 6 4 1 2 ⊗ 2 10 0 0 | 85.4 |
| | | | 6 2 1 4 ⊗ 2 10 0 0 | 11.6 |
| $5/2^-$ | 1186.8 | 1105[a] | 6 4 1 2 ⊗ 2 10 0 0 | 72.6 |
| | | | 5 4 2 2 ⊗ 2 10 0 0 | 13.0 |
| $9/2^-$ | 1790.3 | 1823[a] | 6 4 1 2 ⊗ 2 10 0 0 | 81.5 |
| $11/2^-$ | 2413.4 | 2201[a] | 6 4 1 2 ⊗ 2 10 0 0 | 85.3 |
| | | | 6 3 2 2 ⊗ 2 10 0 0 | 11.6 |
| $13/2^-$ | 1983.9 | 1948[a] | 6 4 1 2 ⊗ 2 10 0 0 | 83.3 |
| $15/2_1^-$ | 2660.3 | 2420[a] | 6 4 1 2 ⊗ 2 10 0 0 | 76.3 |
| | | | 6 3 2 2 ⊗ 2 10 0 0 | 13.2 |
| $15/2_2^-$ | 4397.9 | 4246[a] | 6 3 2 2 ⊗ 2 10 0 0 | 66.9 |
| | | | 6 4 1 2 ⊗ 2 10 0 0 | 12.0 |
| $17/2^-$ | 2034.0 | 1974[a] | 6 4 1 2 ⊗ 2 10 0 0 | 82.9 |
| $21/2_1^-$ | 5956.4 | 5790[a] | 5 4 0 4 ⊗ 2 10 0 0 | 32.2 |
| | | | 4 4 1 4 ⊗ 2 10 0 0 | 21.8 |
| $21/2_2^-$ | 6027.6 | 6224[a] | 5 3 1 4 ⊗ 2 10 0 0 | 56.6 |
| | | | 4 4 1 4 ⊗ 2 10 0 0 | 19.2 |
| $23/2_1^-$ | 6213.2 | 6260[a] | 5 4 0 4 ⊗ 2 10 0 0 | 49.6 |
| | | | 4 4 1 4 ⊗ 2 10 0 0 | 23.0 |
| | | | 5 3 1 4 ⊗ 2 10 0 0 | 18.2 |
| $23/2_2^-$ | 6271.3 | 6493[b] | 6 4 1 2 ⊗ 2 9 0 1 | 53.5 |
| | | | 5 4 2 2 ⊗ 2 9 0 1 | 20.1 |
| $23/2_3^-$ | 6409.1 | 6608[b] | 6 4 1 2 ⊗ 2 9 0 1 | 52.1 |
| | | | 5 4 2 2 ⊗ 2 9 0 1 | 17.8 |
| $25/2_1^-$ | 6258.9 | 6339[b] | 6 4 1 2 ⊗ 2 9 0 1 | 70.4 |
| | | | 6 3 2 2 ⊗ 2 9 0 1 | 15.0 |
| $25/2_2^-$ | 6443.6 | 6481[b] | 6 4 1 2 ⊗ 2 9 0 1 | 74.3 |
| $25/2_3^-$ | 6910.7 | 6858[b] | 5 4 2 2 ⊗ 2 9 0 1 | 35.6 |
| | | | 6 4 1 2 ⊗ 2 9 0 1 | 20.5 |
| $25/2_4^-$ | 6916.6 | 7261[b] | 6 4 1 2 ⊗ 2 9 0 1 | 56.0 |
| | | | 6 3 2 2 ⊗ 2 9 0 1 | 14.0 |
| | | | 5 2 2 2 ⊗ 2 9 0 1 | 12.4 |
| $27/2_1^-$ | 6843.5 | 6972[b] | 6 4 1 2 ⊗ 2 9 0 1 | 67.0 |
| | | | 6 3 2 2 ⊗ 2 9 0 1 | 13.3 |
| $27/2_2^-$ | 7095.4 | 7246[b] | 5 4 2 2 ⊗ 2 9 0 1 | 45.9 |
| | | | 6 4 1 2 ⊗ 2 9 0 1 | 11.2 |
| $27/2_3^-$ | 7560.9 | 7649[b] | 6 4 1 2 ⊗ 2 9 0 1 | 61.7 |
| $29/2_1^-$ | 8357.6 | 8251[b] | 6 4 1 2 ⊗ 2 9 0 1 | 43.4 |

[a]Calculation with the model space $\pi(f_{5/2}, p_{3/2}, p_{1/2}, g_{9/2})$.
[b]$\pi(f_{5/2}, p_{3/2}, p_{1/2}, g_{9/2}) \otimes \nu(g_{9/2}, d_{5/2})$.
[c]$\pi(f_{5/2}, p_{3/2}, p_{1/2}, g_{9/2}) \otimes \nu(g_{9/2}, g_{7/2})$.

the $g_{9/2}$ orbits [11], whereas the $10^+$ states in $^{94}$Ru and $^{96}$Pd nuclei arise from the $\pi(g_{9/2})^n$ ($n = 4$ and 6) configurations, which are not involved with proton core excitation. The level structures from $2^+$ states to $8^+$ ones in $^{92}$Mo, $^{94}$Ru, $^{96}$Pd, and $^{98}$Cd are similar to each other. In these nuclei, the first $2^+$, $4^+$, $6^+$, and $8^+$ states are described by the seniority $\nu = 2$ states in the seniority scheme [65,66]. The angular momenta originate from the coupling of the two unpaired protons in the $g_{9/2}$ orbit.

As shown in Fig. 7(b), similar characteristics are also observed for the odd-$A$ isotones from Nb ($Z = 41$) to Ag ($Z = 47$). The first $13/2^+$ to $21/2^+$ levels may come from the same multiplet that relates to the predominant valence protons in the $\pi g_{9/2}$ orbital with $\nu = 3$. Furthermore, the energy spacings $4^+ \rightarrow 2^+$ ($2^+ \rightarrow 0^+$) in the even-even isotones are very close to the $17/2^+ \rightarrow 13/2^+$ ($13/2^+ \rightarrow 9/2^+$) spacings in the odd-$A$ neighbors, which can be explicated as the weak coupling model, i.e., the coupling of the $g_{9/2}$ valence proton and the neighboring even-even core [26]. The excitation energies of $11/2_1^+$ states are slightly higher than the yrast $13/2_1^+$ levels in $^{91}$Nb, $^{93}$Tc, and $^{95}$Rh nuclei. These levels are the $J^\pi_{max}$ and $J^\pi_{max}$-1 members of the $\pi g_{9/2} \otimes 2^+$ multiplet for the yrast $2^+$ states in $^{90}$Zr, $^{92}$Mo, and $^{94}$Ru, respectively. Similarly, the $17/2^+$ and $21/2^+$ states in the odd-$A$ nuclei might be the numbers of $\pi(g_{9/2}) \otimes 4^+$ and $\pi(g_{9/2}) \otimes 6^+$. As shown in Fig. 7, there are considerable discrepancies between $25/2_1^+$ states in odd-$A$ nuclei and $8_1^+$ states in even-even nuclei which indicate that the intrinsic nucleon excitations are not negligible in high spin levels of the even-even core, and configuration mixing becomes increasingly prominent.

## V. SUMMARY

High spin states of the $^{91}$Nb nucleus were produced via the reactions $^{82}$Se($^{14}$N, $5n$)$^{91}$Nb and $^{76}$Ge ($^{19}$F, $4n$)$^{91}$Nb. The level scheme of the $^{91}$Nb nucleus was extended by adding 30 transitions. The new structure was explicated with shell-model calculations which consider the excitation of the $Z = 38$ (40) subshell closure and the $N = 50$ shell closure, and the calculated results support the experimental angular momentum assignments. Several large $E2$ ($M1$ ) transition probabilities are predicted, which can be considered as a testimony for proton (neutron) core excitations. Additionally, the comparisons of the first excited states from the $46 \leqslant N \leqslant 60$ and $40 \leqslant Z \leqslant 48$ mass region reveal that the $N = 56$ subshell closure significantly affects the level structures of $^{96}$Zr and $^{97}$Nb but almost disappears completely in $Z \geqslant 42$ nuclei.

## ACKNOWLEDGMENTS

We are indebted to all the HI-13 tandem accelerator staff for the smooth operation of the machine. We are grateful to Dr. Q. W. Fan for assistance during target preparation. This work is supported by the National Basic Research Programme of China under Grant No. 2007CB815005; the National Natural Science Foundation of China under Grants No. 11075064, No. 11775098, No. 12075169, and No. U1867210; and the National Key Research and Development Program of China under Grant No. 2018YFA0404403.

TABLE V. The electromagnetic transition probabilities in the $^{91}$Nb nucleus received through the experiment in Ref. [22] are compared with the results of shell-model calculations. Effective values of $e_p = 1.0$ and $e_n = 0.5$ are used for the $B(M1)$ and $B(E2)$ values. For magnetic transitions quenched single-particle $g_s$ factors with $0.7g_s^{\mathrm{free}}$ are assumed.

| $E_\gamma$ (keV) | $J_i^\pi$ | $J_f^\pi$ | $\sigma\lambda$ | $B(\sigma\lambda)_{\mathrm{expt.}}$ $(e^2fm^4/\mu_N{}^2)$ | $B(\sigma\lambda)_{\mathrm{SM}}$ | $\tau(J_i)_{\mathrm{expt.}}$ | $\tau(J_i)_{\mathrm{SM}}$ |
|---|---|---|---|---|---|---|---|
| 1082.0 | $5/2_1^-$ | $1/2_1^-$ | $E2$ | 137.4 | 187.8 | | 13.1 ps |
| 603.5 | $9/2_1^-$ | $5/2_1^-$ | $E2$ | $\downarrow$ 178.0 | 194.5 | $\uparrow$ 2.3 ps | 10.15 ps |
| 193.3 | $13/2_1^-$ | $9/2_1^-$ | $E2$ | $71.1 \pm 3.2$ | 115.6 | $14.4 \pm 0.5$ ns | 12.24 ns |
| 50.1 | $17/2_1^-$ | $13/2_1^-$ | $E2$ | $32.0 \pm 1.9$ | 37.2 | $5.42 \pm 0.18$ μs | 317 μs |
| 2290.4 | $13/2_1^+$ | $9/2_1^+$ | $E2$ | 33.82 | 152.9 | | 0.31 ps |
| 819.2 | $17/2_1^+$ | $13/2_1^+$ | $E2$ | $\uparrow$ 6.64 | 287.8 | | 2.05 ps |
| 356.0 | $21/2_1^+$ | $17/2_1^+$ | $E2$ | $106 \pm 11$ | 100.7 | $1.33 \pm 0.14$ ns | 1.304 ns |
| 1927.0 | $23/2_6^+$ | $19/2_2^+$ | $E2$ | | 5.13 | | 0.89 ps |
| 1981.5 | $25/2_3^+$ | $21/2_2^+$ | $E2$ | | 1.92 | | 0.62 ps |
| 730.4 | $27/2_1^+$ | $23/2_6^+$ | $E2$ | | 0.41 | | 93.5 ps |
| 2054.6 | $27/2_2^+$ | $23/2_1^+$ | $E2$ | | 0.19 | | 0.98 ps |
| 606.7 | $29/2_1^+$ | $25/2_3^+$ | $E2$ | | 132.7 | | 10.53 ps |
| 1062.3 | $25/2_3^+$ | $23/2_3^+$ | $M1$ | | 0.041 | | 1.75 ps |
| 1717.2 | $23/2_2^+$ | $21/2_1^+$ | $M1$ | | 0.0457 | | 0.08 ps |
| 918.7 | $23/2_3^+$ | $21/2_2^+$ | $M1$ | | 0.0177 | | 0.13 ps |
| 184.9 | $29/2_1^+$ | $27/2_1^+$ | $M1$ | | 1.44 | | 21.21 ps |
| 661.9 | $31/2_1^+$ | $29/2_1^+$ | $M1$ | | 2.61 | | 0.12 ps |
| 497.5 | $33/2_2^+$ | $31/2_1^+$ | $M1$ | | 2.67 | | 0.08 ps |


[1] O. Schwentker, J. Dawson, J. Robb, J. Heisenberg, J. Lichtenstadt, C. N. Papanicolas, J. Wise, J. S. McCarthy, L. T. van der Bijl, and H. P. Blok, Phys. Rev. Lett. **50**, 15 (1983).

[2] Z. Q. Li, S. Y. Wang, C. Y. Niu, B. Qi, S. Wang, D. P. Sun, C. Liu, C. J. Xu, L. Liu, P. Zhang, X. G. Wu, G. S. Li, C. Y. He, Y. Zheng, C. B. Li, B. B. Yu, S. P. Hu, S. H. Yao, X. P. Cao, and J. L. Wang, Phys. Rev. C **94**, 014315 (2016).

[3] L. Funke, G. Winter, J. Döring, L. Käubler, H. Prade, R. Schwengner, and E. Will, Nucl. Phys. A **541**, 241 (1992).

[4] E. K. Warburton, J. W. Olness, C. J. Lister, R. W. Zurmühle, and J. A. Becker, Phys. Rev. C **31**, 1184 (1985).

[5] P. Dey, D. Negi, R. Palit, P. C. Srivastava, Md. S. R. Laskar, B. Das, F. S. Babra, S. Bhattacharya, Biswajit Das, K. R. Devi, R. Gala, U. Garg, S. S. Ghugre, E. Ideguchi, S. Kumar, A. Kundu, G. Mukherjee, S. Muralithar, S. Nag, S. Nandi, Neelam, M. Kumar Raja, R. Raut *et al.*Phys. Rev. C **105**, 044307 (2022).

[6] H. Wang, K. Y. Ma, S. Y. Liu, and J. B. Lu, Chin. Phys. C **45**, 094106 (2021).

[7] P. W. Luo, X. G. Wu, H. B. Sun, G. S. Li, C. Y. He, Y. Zheng, C. B. Li, S. P. Hu, Y. H. Wu, H. W. Li, J. J. Liu, J. L. Wang, S. H. Yao, and Scott A. Edwards, Phys. Rev. C **89**, 034318 (2014).

[8] B. A. Brown, P. M. S. Lesser, and D. B. Fossan, Phys. Rev. Lett **34**, 161 (1975).

[9] C. A. Fields, J. J. Kraushaar, R. A. Ristinen, L. E. Samuelson, Nucl. Phys. A **326**, 55 (1979).

[10] P. Singh, R. G. Pillay, J. A. Sheikh, and H. G. Devare, Phys. Rev. C **45**, 2161 (1992).

[11] N. S. Pattabiraman, S. N. Chintalapudi, S. S. Ghugre, B. V. Tirumala Rao, M. L. N. Raju, T. S. Reddy, P. K. Joshi, R. Palit, and H. C. Jain, Phys. Rev. C **65**, 044324 (2002).

[12] S. S. Ghugre and S. K. Datta, Phys. Rev. C **52**, 1881 (1995).

[13] C. Fransen, N. Pietralla, A. P. Tonchev, M. W. Ahmed, J. Chen, G. Feldman, U. Kneissl, J. Li, V. N. Litvinenko, B. Perdue, I. V. Pinayev, H. H. Pitz, R. Prior, K. Sabourov, M. Spraker, W. Tornow, H. R. Weller, V. Werner, Y. K. Wu, and S. W. Yates, Phys. Rev. C **70**, 044317 (2004),

[14] M. Hausmann, A. Jungclaus, E. Galindo, K. P. Lieb, O. Yordanov, I. P. Johnstone, R. Schwengner, A. Dewald, A. Fitzler, O. Möller, G. de Angelis, A. Gadea, T. Martinez, D. R. Napoli, and C. Ur, Phys. Rev. C **68**, 024309 (2003).

[15] S. S. Ghugre, S. B. Patel, M. Gupta, R. K. Bhowmik, and J. A. Sheikh, Phys. Rev. C **47**, 87 (1993).

[16] H. A. Roth, S. E. Arnell, D. Foltescu, O. Skeppstedt, J. Blomqvist, A. Nilsson, T. Kuroyanagi, S. Mitarai, and J. Nyberg, Phys. Rev. C **50**, 1330 (1994).

[17] A. Jungclaus, D. Kast, K. P. Lieb, C. Teich, M. Weiszflog, T. Härtlein, C. Ender, F. Köck, D. Schwalm, I. P. Johnstone, J. Reif, R. Schwengner, R. Peusquens, A. Dewald, J. Eberth, H. G. Thomas, M. Górska, and H. Grawe, Phys. Rev. C **60**, 014309 (1999).

[18] F. Ghazi Moradi, C. Qi, B. Cederwall, A. Atac, T. Bäck, R. Liotta, M. Doncel, A. Johnson, G. de France, E. Clément, A. Dijon, R. Wadsworth, T. W. Henry, A. J. Nichols, H. Al-Azri, J. Nyberg, A. Gengelbach, T. üyük, B. M. Nyakó, J. Timár, D. Sohler, Zs. Dombrádi, I. Kuti *et al.*, Phys. Rev. C **89**, 014301 (2014).

[19] H. Mach, A. Korgul, M. Górska, H. Grawe, I. Matea, M. Stănoiu, L. M. Fraile, Yu. E. Penionzkevich, F. De Oliviera Santos, D. Verney, S. Lukyanov, B. Cederwall, A. Covello, Z. Dlouhý, B. Fogelberg, G. De France, A. Gargano, G. Georgiev, R. Grzywacz, A. F. Lisetskiy, J. Mrazek, F. Nowacki *et al.*, Phys. Rev. C **95**, 014313 (2017).

[20] Dennis L. Matthews, Terry P. Lindsey, Masahiro Koike, and C. Fred Moore, Phys. Rev. C **4**, 1876 (1971).

[21] M. S. Zisman and B. G. Harvey, Phys. Rev. C **4**, 1809 (1971).

[22] B. A. Brown, P. M. S. Lesser, and D. B. Fossan, Phys. Rev. C **13**, 1900 (1976).
[23] O. Häusser, I. S. Towner, T. Faestermann, H. R. Andrews, J. R. Beene, D. Horn, D. Ward, C. Broude, Nucl. Phys. A **293**, 248 (1977).
[24] M. Piiparinen, A. Ataç, J. Blomqvist, G. B. Hagemann, B. Herskind, R. Julin, S. Juutinen, A. Lampinen, J. Nyberg, G. Sletten, P. Tikkanen, S. Törrmänen, A. Virtanen, and R. Wyss, Nucl. Phys. A **605**, 191 (1996).
[25] Y. Zheng, Y. H. Wu, X. G. Wu, C. B. Li, L. H. Zhu, T. X. Li, P. W. Luo, G. S. Li, C. Y. He, H. W. Li, S. P. Hu, J. J. Liu, J. L. Wang, S. H. Yao, Q. M. Chen, J. Zhong, J. B. Lu, K. Y. Ma, and D. Yang, Phys. Rev. C **100**, 014325 (2019).
[26] E. A. Stefanova, R. Schwengner, J. Reif, H. Schnare, F. Dönau, M. Wilhelm, A. Fitzler, S. Kasemann, P. von Brentano, and W. Andrejtscheff, Phys. Rev. C **62**, 054314 (2000).
[27] G. J. Kumbartzki, K.-H. Speidel, N. Benczer-Koller, D. A. Torres, Y. Y. Sharon, L. Zamick, S. J. Q. Robinson, P. Maier-Komor, T. Ahn, V. Anagnostatou, Ch. Bernards, M. Elvers, P. Goddard, A. Heinz, G. Ilie, D. Radeck, D. Savran, V. Werner, and E. Williams, Phys. Rev. C **85**, 044322 (2012).
[28] Y. H. Wu, J. B. Lu, Z. Ren, G. J. Fu, J. Li, K. Y. Ma, Y. J. Ma, X. G. Wu, Y. Zheng, C. B. Li, and J. Wen, Phys. Rev. C **105**, 034344 (2022).
[29] B. Brown and W. Rae, Nucl. Data Sheets **120**, 115 (2014).
[30] A. Hosaka, K.-I. Kubo and H. Toki, Nucl. Phys. A **444**, 76 (1985).
[31] X. Ji and B. H. Wildenthal, Phys. Rev. C **37**, 1256 (1988).
[32] D. Gloeckner, Nucl. Phys. A **253**, 301 (1975).
[33] F. Serduke, R. Lawson, and D. Gloeckner, Nucl. Phys. A **256**, 45 (1976).
[34] A. Negret and B. Singh, Nucl. Data Sheets **124**, 1 (2015)
[35] D. Pantelica, I. Gh. Stefan, N. Nica, M.-G. Porquet, G. Duchene, A. Astier, S. Courtin, I. Deloncle, F. Hoellinger, A. Bauchet, N. Buforn, L. Donadille, O. Dorvaux, J. Duprat, B. J. P. Gall, C. Gautherin, T. Kutsarova, S. Lalkovski, R. Lucas, M. Meyer, A. Minkova, A. Prévost *et al.*, Phys. Rev. C **72**, 024304 (2005).
[36] S. Ansari, J. M. Régis, J. Jolie, N. Saed-Samii, N. Warr, W. Korten, M. Zielińska, M. D. Salsac, A. Blanc, M. Jentschel, U. Köster, P. Mutti, T. Soldner, G. S. Simpson, F. Drouet, A. Vancraeyenest, G. de France, E. Clément, O. Stezowski, C. A. Ur *et al.*, Phys. Rev. C **96**, 054323 (2017).
[37] M. K. Kabadiyski, C. J. Gross, A. Harder, K. P. Lieb, D. Rudolph, M. Weiszflog, J. Altmann, A. Dewald, J. Eberth, T. Mylaeus, H. Grawe, J. Heese, and K.-H. Maier, Phys. Rev. C **50**, 110 (1994).
[38] P. Paradis, G. Lamoureux, R. Lecomte, and S. Monaro, Phys. Rev. C **14**, 835 (1976).
[39] A. Esmaylzadeh, V. Karayonchev, K. Nomura, J. Jolie, M. Beckers, A. Blazhev, A. Dewald, C. Fransen, R.-B. Gerst, G. Häfner, A. Harter, L. Knafla, M. Ley, L. M. Robledo, R. Rodríguez-Guzmán, and M. Rudigier, Phys. Rev. C **104**, 064314 (2021).
[40] E. Browne, Nucl. Data Sheets **82**, 379 (1997).
[41] C. M. Baglin, Nucl. Data Sheets **113**, 2187 (2012).
[42] D. Abriola and A. A. Sonzogni, Nucl. Data Sheets **107**, 2423 (2006).
[43] D. Abriola and A. A. Sonzogni, Nucl. Data Sheets **109**, 2501 (2008).
[44] B. Singh and Z. Q. Hu, Nucl. Data Sheets **98**, 335 (2003).
[45] B. Singh, Nucl. Data Sheets **109**, 297 (2008).
[46] D. De Frenne, Nucl. Data Sheets **110**, 1745 (2009).
[47] J. Blachot, Nucl. Data Sheets **108**, 2035 (2007).
[48] N. Mărginean, D. Bucurescu, C. Rossi Alvarez, C. A. Ur, L. D. Skouras, L. P. Johnstone, D. Bazzacco, S. Lunardi, G. de Angelis, M. Axiotis, E. Farnea, A. Gadea, M. Ionescu-Bujor, A. Iordăchescu, W. Krolas, Th. Kröll, S. M. Lenzi, T. Martinez, R. Mărginean, R. Menegazzo, D. R. Napoli, P. Pavan, M. De Poli *et al.*Phys. Rev. C **67**, 061301(R) (2003).
[49] M. Palacz, J. Nyberg, H. Grawe, K. Sieja, G. de Angelis, P. Bednarczyk, A. Blazhev, D. Curien, Z. Dombradi, O. Dorvaux, J. Ekman, J. Gałkowski, M. Górska, J. Iwanicki, G. Jaworski, J. Kownacki, J. Ljungvall, M. Moszyński, F. Nowacki, D. Rudolph *et al.*, Phys. Rev. C **86**, 014318 (2012).
[50] W. F. Piel, Jr., G. Scharff-Goldhaber, C. J. Lister and B. J. Varley, Phys. Rev. C **28**, 209 (1983).
[51] A. Blazhev, M. Górska, H. Grawe, J. Nyberg, M. Palacz, E. Caurier, O. Dorvaux, A. Gadea, F. Nowacki, C. Andreoiu, G. de Angelis, D. Balabanski, Ch. Beck, B. Cederwall, D. Curien, J. Döring, J. Ekman, C. Fahlander, K. Lagergren, J. Ljungvall, M. Moszyński *et al.*, Phys. Rev. C **69**, 064304 (2004).
[52] D. De Frenne and A. Negret, Nucl. Data Sheets **109**, 943 (2008).
[53] J. Blachot, Nucl. Data Sheets **90**, 135 (2000).
[54] A. Jungclaus, K. P. Lieb, C. J. Gross, J. Heese, D. Rudolph, D. J. Blumenthal, P. Chowdhury, P. J. Ennis, C. J. Lister, Ch. Winter, J. Eberth, S. Skoda, M. A. Bentley, W. Gelletly, and B. J. Varley, Z. Phys. A **340**, 125 (1991).
[55] B. Singh, Nucl. Data Sheets **114**, 1 (2013).
[56] Coral M. Baglin, Nucl. Data Sheets **114**, 1293 (2013).
[57] Coral M. Baglin, Nucl. Data Sheets **112**, 1163 (2011).
[58] S. K. Basu and G. Mukherjee, Nucl. Data Sheets **111**, 2555 (2010).
[59] N. Nica, Nucl. Data Sheets **111**, 525 (2010).
[60] E. Browne, J. K. Tuli, Nucl. Data Sheets **145**, 25 (2017).
[61] J. B. Lachot, Nucl. Data Sheets **83**, 1 (1998).
[62] D. De Frenne, Nucl. Data Sheets **110**, 2081 (2009).
[63] D. De Frenne and E. Jacobs, Nucl. Data Sheets **105**, 775 (2005).
[64] J. Blachot, Nucl. Data Sheets **109**, 1383 (2008).
[65] G. Racah, Phys. Rev. **62**, 438 (1942).
[66] G. Racah, Phys. Rev. **63**, 367 (1943).